Dynamical quantum phase transitions in the Kitaev honeycomb model

Markus Schmitt* and Stefan Kehrein
Institut für Theoretische Physik, Georg-August-Universtät Göttingen, D-37077 Göttingen, Germany
(Received 20 May 2015; published 10 August 2015)

The notion of a dynamical quantum phase transition (DQPT) was recently introduced [Heyl *et al.*, Phys. Rev. Lett. **110**, 135704 (2013)] as the nonanalytic behavior of the Loschmidt echo at critical times in the thermodynamic limit. In this work the quench dynamics in the ground state sector of the two-dimensional Kitaev honeycomb model is studied regarding the occurrence of DQPTs. For general two-dimensional systems of BCS type it is demonstrated how the zeros of the Loschmidt echo coalesce to areas in the thermodynamic limit, implying that DQPTs occur as discontinuities in the second derivative. In the Kitaev honeycomb model DQPTs appear after quenches across a phase boundary or within the massless phase. In the 1d limit of the Kitaev honeycomb model it becomes clear that the discontinuity in the higher derivative is intimately related to the higher dimensionality of the nondegenerate model. Moreover, there is a strong connection between the stationary value of the rate function of the Loschmidt echo after long times and the occurrence of DQPTs in this model.

DOI: 10.1103/PhysRevB.92.075114 PACS number(s): 64.70.Tg, 05.70.Ln, 05.30.Rt

I. INTRODUCTION

Recent advances in experimental techniques allow us to realize closed quantum systems with cold atomic gases in optical traps [1,2]. These setups are precisely controllable and the unitary time evolution of the systems can be resolved such that the dynamics is experimentally accessible under well-known conditions. Motivated by the new experimental possibilities a lot of theoretical research on the nonequilibrium dynamics of quantum systems has been conducted in the past years. In these theoretical investigations a common protocol for driving a system out of equilibrium is called *quantum quench*. Considering a parametrized Hamiltonian $H(\alpha)$, where the parameter typically corresponds to some external field strength in the experimental setup, the system is initially assumed to be in equilibrium with regard to some value α_i of the parameter. Then, the parameter is suddenly *quenched* to a different final value α_f driving the system out of equilibrium and inducing a nontrivial time evolution.

Studying the quench dynamics of a quantum many-body system, Heyl *et al.* [3] pointed out the close formal similarity of the canonical partition function of an equilibrium system, $Z(\beta) = \mathrm{tr}(e^{-\beta H})$, and the return amplitude

$$\mathcal{G}(t) = \langle\psi_i|e^{-iHt}|\psi_i\rangle \tag{1}$$

of a time-evolved state, suggesting the possibility of critical behavior in the time evolution in analogy to equilibrium phase transitions. It is known that in the thermodynamic limit the zeros of a partition function coalesce to lines in the complex temperature plane and the equilibrium phase transition is marked by the intersection of the zero line with the real temperature axis [4]. Heyl *et al.* found that in the case of the transverse field Ising model the boundary partition function

$$Z(z) = \langle\psi_i|e^{-zH}|\psi_i\rangle \tag{2}$$

has zeros in the complex time plane, which accordingly coalesce to lines in the thermodynamic limit. These lines cross the real time axis after quenching the external field across the quantum critical point inducing nonanalyticities in the rate function of the Loschmidt echo

$$\begin{aligned} r(t) &= -\lim_{N\to\infty}\frac{1}{N}\ln|\langle\psi_i|e^{-iHt}|\psi_i\rangle|^2 \\ &= -\lim_{N\to\infty}\frac{1}{N}\ln\mathcal{L}(t) \end{aligned} \tag{3}$$

at equidistant critical times t_n^*. Heyl *et al.* denote this nonanalytic behavior at critical times in the thermodynamic limit as a dynamical quantum phase transition (DQPT). They showed that in experiment the DQPT would be observable by measuring the work distribution function of a double quench; in particular, the Loschmidt echo $\mathcal{L}(t) = |\langle\psi_i|e^{-iHt}|\psi_i\rangle|^2$ is the probability of performing no work.

These findings triggered further work aiming at a better understanding of the phenomenon. By considering an additional integrability-breaking interaction in the transverse field Ising chain it was demonstrated that DQPTs are not a peculiarity specific to integrable models, but are stable against some nonintegrable perturbations [5,6]. Moreover, the signature of DQPTs was found in higher-dimensional systems, namely, in two-dimensional topological insulators [7] and effectively infinite dimensions using DMFT [8]. It was observed in various cases that DQPTs are not necessarily connected to quenching across a quantum critical point [8–11]; however, there seems to be a strong connection to topological phase transitions [7,12]. Canovi *et al.* [8] detected coexisting solutions for so called generalized expectation values in postquench dynamics and, therefore, they introduced the notion of a first-order dynamical phase transition. This could be a way to classify dynamical phase transitions. Furthermore, zeros in the oscillations of the Schmidt gap were related to DQPTs [13] and a close connection between the analytic behavior of $r(t)$ in the complex plane and its long time limit is conjectured [14].

In this work we study quench dynamics in the Kitaev honeycomb model [15] regarding dynamical quantum phase transitions. The model features a rich phase diagram comprising an extended gapless phase, anyonic excitations, and topological order. Moreover, it is a rare example of a Jordan-Wigner-solvable model in two dimensions [16,17]. As such it has been

*markus.schmitt@theorie.physik.uni-goettingen.de

studied extensively under various aspects. In this paper we restrict the discussion to the dynamics in the ground state sector.

The dynamics of gapped two-dimensional two-band systems was already studied by Vajna and Dóra with focus on a connection between DQPTs and topological phases [7]. In the presence of a magnetic field the Kitaev model acquires topological order and becomes a system of the same family, albeit being a spin model. In that case we find the behavior in accordance with their results; namely, DQPTs occur after quenches across the boundary between phases with different Chern number. However, the focus of this work lies on quenching between the topologically trivial phases in the absence of a magnetic field. Similarly to their results we find DQPTs as discontinuities in the second derivative, which is inherent to the higher dimensionality of the system, and we elaborate on the relevance of the complex zeros of the dynamical partition function in this context. Moreover, we discuss a remarkable observation regarding the long time behavior of the Loschmidt echo. If no DQPTs occur in the postquench dynamics, then, although the approached stationary state is always an excited state, the long time limit of the Loschmidt echo is given by the fidelity, i.e., the overlap of the initial state with the ground state of the quenched Hamiltonian. This, however, does not hold if the dynamics exhibits DQPTs.

The rest of this paper is organized as follows: In Sec. II the way of solving the model using Jordan-Wigner transformation is sketched and the phase diagram is introduced. Furthermore, the expressions for the dynamical free energy are derived. In Sec. III the zeros of the dynamical partition function in the complex time plane are treated assuming a general BCS-type Hamiltonian, yielding the criteria for the occurrence of DQPTs and the order of the corresponding nonanalyticity. Finally, the zeros of the partition function and the real time evolution are studied explicitly for the Kitaev model in Sec. IV, and two interesting limits are taken into account as well as ramping as an alternative protocol and the quenching with an additional magnetic field.

II. THE KITAEV HONEYCOMB MODEL

A. The model

The Kitaev honeycomb model is defined by the Hamiltonian

$$H(\vec{J}) = -\sum_{\alpha\in\{x,y,z\}}\sum_{\alpha\text{-links}} J_\alpha \sigma_j^\alpha \sigma_k^\alpha, \tag{4}$$

which describes a spin-1/2 system with the spins located on the vertices (labeled by j,k) of a honeycomb lattice as depicted in Fig. 1 [15]. In this paper we assume the lattice spacing to equal unity. It has been shown [17] that for the above Hamiltonian one can find a Jordan-Wigner contour, which after identifying a conserved Z_2 operator [18] and switching to momentum space yields a BCS-type Hamiltonian

$$H(\vec{J}) = \sum_{\vec{k}}\left[\frac{\epsilon_{\vec{k}}(\vec{J})}{2}(d_{\vec{k}}^\dagger d_{\vec{k}} - d_{-\vec{k}} d_{-\vec{k}}^\dagger) + \frac{\Delta_{\vec{k}}(\vec{J})}{2}(d_{\vec{k}}^\dagger d_{-\vec{k}}^\dagger + d_{-\vec{k}} d_{\vec{k}})\right] \tag{5}$$

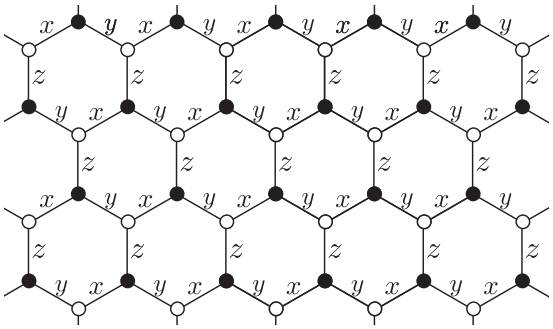

FIG. 1. Lattice of the Kitaev honeycomb model given by Eq. (4). Spin-1/2 degrees of freedom are sitting on the vertices of a honeycomb lattice. The nearest neighbor interaction depends on the link type (x,y, or z).

with

$$\begin{aligned}\epsilon_{\vec{k}}(\vec{J}) &= 2[J_z + J_x\cos(k_x) + J_y\cos(k_y)],\\ \Delta_{\vec{k}}(\vec{J}) &= 2[J_x\sin(k_x) + J_y\sin(k_y)].\end{aligned} \tag{6}$$

This Hamiltonian can be diagonalized by a Bogoliubov transformation

$$\begin{pmatrix} a_{\vec{k}}^{\vec{J}} \\ a_{-\vec{k}}^{\vec{J}\dagger}\end{pmatrix} = \begin{pmatrix} u_{\vec{k}}(\vec{J}) & v_{\vec{k}}(\vec{J}) \\ -v_{\vec{k}}(\vec{J})^* & u_{\vec{k}}(\vec{J})^*\end{pmatrix}\begin{pmatrix} d_{\vec{k}} \\ d_{-\vec{k}}^\dagger\end{pmatrix}, \tag{7}$$

where

$$\begin{aligned} u_{\vec{k}}(\vec{J}) &= \sqrt{\frac{1}{2}\left(1 + \frac{\epsilon_{\vec{k}}(\vec{J})}{E_{\vec{k}}(\vec{J})}\right)},\\ v_{\vec{k}}(\vec{J}) &= \mathrm{sgn}[\Delta_{\vec{k}}(\vec{J})]\sqrt{\frac{1}{2}\left(1 - \frac{\epsilon_{\vec{k}}(\vec{J})}{E_{\vec{k}}(\vec{J})}\right)}\end{aligned} \tag{8}$$

(see Appendix A for details). Plugging the transformation into Eq. (5) yields the diagonal Hamiltonian

$$H(\vec{J}) = \sum_{\vec{k}\in K}\frac{E_{\vec{k}}(\vec{J})}{2}(a_{\vec{k}}^\dagger a_{\vec{k}} - a_{-\vec{k}} a_{-\vec{k}}^\dagger) \tag{9}$$

with spectrum

$$E_{\vec{k}}(\vec{J}) = \sqrt{\epsilon_{\vec{k}}(\vec{J})^2 + \Delta_{\vec{k}}(\vec{J})^2}. \tag{10}$$

The Hamiltonian splits into a sum over $\vec{k}$ sectors, i.e., a sum over $\vec{k}\in K$, where K is a subset of the Brillouin zone such that $\forall\vec{k}\in K$, $-\vec{k}\notin K$. A possible choice is one half of the Brillouin zone, e.g., all $\vec{k}$ with $k_x > 0$ [19].

The spectrum has roots at

$$\begin{aligned} k_x &= \pm\arccos\left(\frac{J_y^2 - J_x^2 - J_z^2}{2J_xJ_z}\right),\\ k_y &= \mp\arccos\left(\frac{J_x^2 - J_y^2 - J_z^2}{2J_yJ_z}\right)\end{aligned} \tag{11}$$

if $|J_\alpha| < |J_\beta| + |J_\gamma|$, where (α,β,γ) is any permutation of (x,y,z). We will in the following only consider nonnegative J_α on the $J_x + J_y + J_z = 1$ plane. In this section the above result

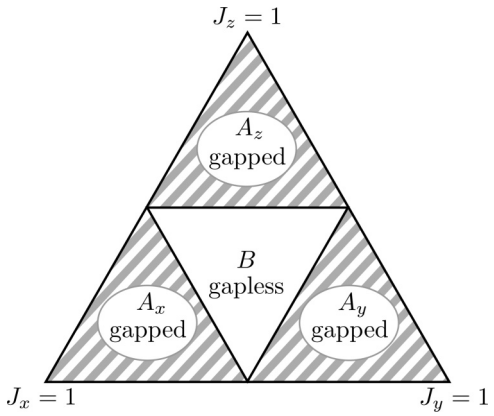

FIG. 2. Phase diagram of the Kitaev model in the $J_x + J_y + J_z = 1$ plane, where $J_\alpha \geqslant 0$. The gapless phase B is surrounded by three gapped phases A_α, where $J_\alpha > J_\beta + J_\gamma$.

on the gappedness of the spectrum corresponds to a phase diagram as depicted in Fig. 2. The gapless phase B at the center of the diagram is surrounded by three distinct gapped phases [15] A_x, A_y, and A_z, where $J_x > J_y + J_z$, $J_y > J_x + J_z$, or $J_z > J_y + J_x$, respectively.

In the presence of a magnetic field $\vec{h}$ the spin Hamiltonian (4) becomes

$$H(\vec{J},\vec{h}) = -\sum_{\alpha\in\{x,y,z\}}\left(\sum_{\alpha\text{-links}} J_\alpha \sigma_j^\alpha \sigma_k^\alpha + \sum_j h_\alpha \sigma_j^\alpha\right) \quad (12)$$

and the additional term opens a gap also in the B phase. Moreover, the B phase becomes topologically nontrivial with Chern number $\nu = \pm 1$, whereas the A_α phases remain trivial with $\nu = 0$ [15]. At $J_x = J_y = J_z = J$ there exists a diagonal form of the Hamiltonian even with nonzero magnetic field [15] and the spectrum reads

$$E_{\vec{k}}(J,h) = \sqrt{\tilde{\epsilon}_{\vec{k}}(J,\kappa)^2 + |\tilde{\Delta}_{\vec{k}}(J,\kappa)|^2} \quad (13)$$

with $\tilde{\epsilon}_{\vec{k}}(J,\kappa) = \epsilon_{\vec{k}}(\vec{J})$, $\vec{J} = (J,J,J)^T$, and

$$\tilde{\Delta}_{\vec{k}}(J,\kappa) = \Delta_{\vec{k}}(\vec{J}) + 4i\kappa[\sin(k_x) - \sin(k_y) + \sin(k_y - k_x)], \quad (14)$$

where $\kappa \sim \frac{h_x h_y h_z}{J^2}$. Through a Bogoliubov transformation (see Appendix A) this maps to

$$H(J,\kappa) = \sum_{\vec{k}\in K}\left[\frac{\tilde{\epsilon}_{\vec{k}}(J,\kappa)}{2}(d_{\vec{k}}^\dagger d_{\vec{k}} - d_{-\vec{k}} d_{-\vec{k}}^\dagger) + \frac{\tilde{\Delta}_{\vec{k}}(J,\kappa)}{2} d_{\vec{k}}^\dagger d_{-\vec{k}}^\dagger + \frac{\tilde{\Delta}_{\vec{k}}(J,\kappa)^*}{2} d_{-\vec{k}} d_{\vec{k}}\right]. \quad (15)$$

This case will be studied in Sec. IV F. Before, we will stick to the case without magnetic field, i.e., real valued $\epsilon_{\vec{k}}$ and $\Delta_{\vec{k}}$.

B. Postquench dynamics

In order to study the dynamics in the Kitaev honeycomb model we will consider situations where the system is initially, at $t < 0$, prepared in the ground state of $H(\vec{J}_0)$, i.e., $H(\vec{J}_0)|\psi_i\rangle = E_{\mathrm{GS}}|\psi_i\rangle$. In terms of the free fermion degrees of freedom the initial state is the vacuum: $a_{\vec{k}}^{\vec{J}_0}|\psi_i\rangle = a_{\vec{k}}^{\vec{J}_0}|0;\vec{J}_0\rangle = 0$. At $t = 0$ the parameter is quenched to its final value $\vec{J}_1$, such that for $t > 0$ the time-evolved state is $|\psi(t)\rangle = e^{-iH(\vec{J}_1)t}|\psi_i\rangle$. Making use of the Bogoliubov transformation the initial state can be expressed in terms of the final free fermions, which diagonalize $H(\vec{J}_1)$:

$$|\psi_i\rangle = \mathcal{N}^{-1}\prod_{\vec{k}\in K}\left(1 + B_{\vec{k}}(\vec{J}_0,\vec{J}_1) a_{\vec{k}}^{\vec{J}_1\dagger} a_{-\vec{k}}^{\vec{J}_1\dagger}\right)|0;\vec{J}_1\rangle. \quad (16)$$

Here,

$$B_{\vec{k}}(\vec{J}_0,\vec{J}_1) \equiv \frac{V_{\vec{k}}(\vec{J}_0,\vec{J}_1)}{U_{\vec{k}}(\vec{J}_0,\vec{J}_1)} = \frac{u_{\vec{k}}(\vec{J}_0)v_{\vec{k}}(\vec{J}_1) - u_{\vec{k}}(\vec{J}_1)v_{\vec{k}}(\vec{J}_0)}{u_{\vec{k}}(\vec{J}_1)u_{\vec{k}}(\vec{J}_0) + v_{\vec{k}}(\vec{J}_1)v_{\vec{k}}(\vec{J}_0)} \quad (17)$$

and the normalization constant

$$\mathcal{N}^2 \equiv \prod_{\vec{k}\in K}(1 + B_{\vec{k}}(\vec{J}_0,\vec{J}_1)^2) \quad (18)$$

were introduced and $|0;\vec{J}_1\rangle$ is the ground state of $H(\vec{J}_1)$. A more detailed derivation is given in Appendix A.

For the sake of brevity and lucidity we will in the following refrain from dragging along the dependencies on $\vec{J}_0$ and $\vec{J}_1$ explicitly, i.e., identify $B_{\vec{k}} \equiv B_{\vec{k}}(\vec{J}_0,\vec{J}_1)$ and $a_{\vec{k}} \equiv a_{\vec{k}}^{\vec{J}_1}$.

Using (16) to compute the dynamical partition function we obtain

$$Z(z) = \langle\psi_i|e^{-zH}|\psi_i\rangle \quad (19)$$

$$= \prod_{\vec{k}\in K}\frac{1 + B_{\vec{k}}^2 e^{-2E_{\vec{k}}(\vec{J}_1)z}}{1 + B_{\vec{k}}^2}. \quad (20)$$

The dynamical partition function has large deviation form $Z(z) \sim e^{-Nf(z)}$, where N is the system size. Thus, in the thermodynamic limit only the rate function, or dynamical free energy density,

$$f(z) = -\lim_{N\to\infty}\frac{1}{N}\ln[Z(z)] \quad (21)$$

is well defined.

III. ZEROS OF THE PARTITION FUNCTION AND CRITICAL TIMES

A. General aspects

From the study of equilibrium phase transitions it is known that a very insightful approach is to consider the zeros of the partition function in the complex temperature or complex magnetization plane, respectively [4,20,21]. In the thermodynamic limit the zeros of the partition function coalesce to lines or areas in the complex plane, which mark the critical points when approaching the real temperature (magnetization) axis. Analogous reasoning has proven useful in the study of dynamical quantum phase transitions [3,7].

In particular, an interesting analogy to electrodynamics allows us to characterize the dynamical phase transition through the density of zeros of the dynamical partition function in the complex time plane. The starting point is the observation

that the dynamical partition function (19) is an entire function of z and can as such, according to the Weierstrass factorization theorem, be written as

$$Z(z) = e^{h(z)} \prod_{j\in\mathcal{I}} \left(1 - \frac{z}{z_j}\right), \tag{22}$$

where $\mathcal{I}$ is some discrete index set, $z_j \in \mathbb{C}$ are the zeros, and $h(z)$ is an entire function [3]. With this, the dynamical free energy density reads

$$f(z) = -\lim_{N\to\infty} \frac{1}{N}\left[h(z) + \sum_{j\in\mathcal{I}} \ln\left(1 - \frac{z}{z_j}\right)\right]. \tag{23}$$

From this expression it becomes clear that any nonanalytic behavior of the dynamical free energy can only occur at or in the vicinity of the zeros of the dynamical partition function z_j. Since we are interested in nonanalyticities, we will in the following ignore the contribution of $h(z)$ and only consider the singular part

$$f^s(z) = -\lim_{N\to\infty} \frac{1}{N} \sum_{j\in\mathcal{I}} \ln\left(1 - \frac{z}{z_j}\right). \tag{24}$$

In the thermodynamic limit the sum becomes an integral over some continuous variable $x \in X$, where $X \subseteq \mathbb{R}^n$ is a region corresponding to the previously used index set $\mathcal{I}$, and the zeros become a function of this variable $\tilde{z}(x)$, such that

$$f^s(z) = -\int_X dx \ln\left(1 - \frac{z}{\tilde{z}(x)}\right). \tag{25}$$

A transformation of the integration variable yields

$$f^s(z) = -\int_{z(X)} d\tilde{z}\rho(\tilde{z}) \ln\left(1 - \frac{z}{\tilde{z}}\right), \tag{26}$$

where the Jacobian determinant $\rho(\tilde{z})$ can be interpreted as the density of zeros in the complex plane [22]. Moreover, setting $\rho(z) \equiv 0$ for $z \notin z(X)$ allows us to extend the integration domain to the full complex plane. We will now discuss the real part

$$\phi(z) = \mathrm{Re}[f^s(z)] = -\int_{\mathbb{C}} d\tilde{z}\rho(\tilde{z}) \ln\left|1 - \frac{z}{\tilde{z}}\right|. \tag{27}$$

We will later see that the Loschmidt echo on the real time axis is directly given by $\phi(t)$. For $z = u + iv$ with $u, v \in \mathbb{R}$ $\ln|z|$ is the Green's function of the Laplacian $\Delta_{2D} = \frac{\partial^2}{\partial u^2} + \frac{\partial^2}{\partial v^2}$, i.e.,

$$\Delta_{2D}\phi(z) = -2\pi\rho(z). \tag{28}$$

In other words, the real part of the dynamical free energy density can be interpreted as the electrostatic potential $\phi(z)$ produced by a charge density $\rho(z)$ in two dimensions and the question of the behavior of the free energy at critical points becomes the question of the behavior of the electrostatic potential at surfaces. If the zeros form lines in the complex plane, this allows us to deduce the order of the phase transition directly from the density of zeros at or in the vicinity of the physically relevant z [21].

Although the zeros can form areas in the complex plane these areas do not cover the physical axis in the case of equilibrium phase transitions. This is to be expected, since in thermal phase transitions there is typically only one critical point in the physical parameter [22]. However, as we will see in the following section, this is possible in the case of dynamical phase transitions. Thus, consider the situation as depicted in Fig. 3. The density of zeros is given by $\rho_1(z)$ and $\rho_2(z)$ in area I and II, respectively, and at the boundary there is a discontinuous change in the density of zeros. Assume the electric potentials $\phi_i(z)$, $i = 1,2$, solve the Laplace equation (28) with the corresponding density $\rho_i(z)$. With this a global solution is

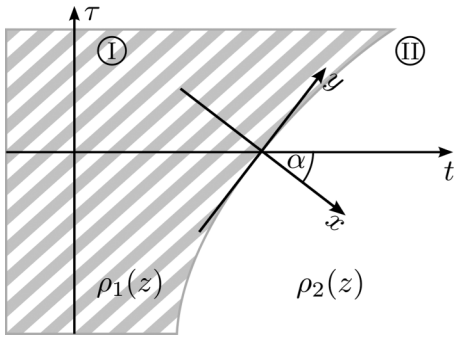

FIG. 3. Schematic picture of the surface separating two densities of zeros in the complex plane and the relevant coordinate frames for determining the behavior of $\phi(z)$ [Eq. (27)] along the real time axis.

$$\phi(z) = \begin{cases} \phi_1(z), & z \in I, \\ \phi_2(z), & z \in II. \end{cases} \tag{29}$$

Let us now focus on the behavior of $\phi(z)$ at the intersection of the boundary with the real time axis. It is known from electrostatics that the curl of the electric field vanishes. If we choose the x-y-coordinate frame as indicated in Fig. 3 this implies (through Stokes' theorem) that on the boundary

$$\frac{\partial^2}{\partial y^2}\phi_1(z) - \frac{\partial^2}{\partial y^2}\phi_2(z) = 0. \tag{30}$$

Since we are interested in the behavior of $\phi(z)$ in the real time axis, we transform to t-y' coordinates,

$$\begin{aligned} t &= \frac{x}{\cos\alpha} + \frac{y}{\sin\alpha}, \\ y' &= y. \end{aligned} \tag{31}$$

With the Laplace equation (28) this yields

$$(\cos\alpha)^{-2}\frac{\partial^2}{\partial t^2}\phi_i(z) + (1 + \sin\alpha^{-1})^2\frac{\partial^2}{\partial y'^2}\phi_i(z) = -2\pi\rho_i(z), \tag{32}$$

and, consequently,

$$\frac{\partial^2}{\partial t^2}[\phi_1(z) - \phi_2(z)] = -2\pi(\cos\alpha)^2[\rho_1(z) - \rho_2(z)]. \tag{33}$$

This means that if an area of zeros of the partition function overlaps the real time axis, the second derivative of the real part of the free energy is discontinuous.

B. 2d BCS-type models

In the Kitaev honeycomb model (and general BCS-type models) the partition function is given by (20); i.e., the zeros in the complex plane are given by

$$z_n(\vec{k}) = \frac{1}{2E_{\vec{k}}}\left[\ln\left(B_{\vec{k}}^2\right) + i\pi(2n+1)\right], \quad n \in \mathbb{Z}. \tag{34}$$

At this point it becomes obvious that in the thermodynamic limit the double product over k_x and k_y in Eq. (20) leads to dense areas of zeros in the complex plane, since, generally, $\partial_{k_x} z_n(\vec{k}) \neq \pm\partial_{k_y} z_n(\vec{k})$. These areas of zeros cover parts of the real time axis ($z = it$) if $\mathrm{Re}[z_n(\vec{k})] = 0$, i.e., if

$$\exists \vec{q} \in K \text{ such that } B_{\vec{q}}^2 = 1. \tag{35}$$

Dubbing the $B_{\vec{q}}^2 = 1$ isoline $\mathcal{B}_1 \subset K$, there are intervals

$$T_n^* = \frac{(2n+1)\pi}{2E_{\mathcal{B}_1}}, \quad n \in \mathbb{Z}, \tag{36}$$

on the real time axis, which are covered by areas of zeros. The beginning t_n^b and end points t_n^e of the intervals T_n^* are determined through Eq. (36) by the maximum and minimum, respectively, of $E_{\vec{k}}$ on the domain given by $|B_{\vec{k}}| = 1$. If the spectrum of the final Hamiltonian is gapped, the beginnings and end points of two consecutive intervals T_n^* and T_{n+1}^* are equidistant with $t_{n+1}^b - t_n^b = \frac{\pi}{2E_{\vec{q}_b}}$ and $t_{n+1}^e - t_n^e = \frac{\pi}{2E_{\vec{q}_e}}$, where $\vec{q}_{b/e}$ are momenta minimizing/maximizing $E_{\vec{k}}$ on the domain given by $|B_{\vec{k}}| = 1$. The length of the single intervals T_n^* increases linearly with n. However, if the spectrum is gapless, all those intervals extend to infinity.

The condition (35) allows for a physical interpretation; namely, the occurrence of DQPTs is through a continuity argument related to nonthermal mode occupation [3]. In BCS-type models the mode occupation is given by

$$\langle n_{\vec{k}} \rangle \equiv \langle a_{\vec{k}}^\dagger a_{\vec{k}} \rangle = \sin^2(\arctan B_{\vec{k}}). \tag{37}$$

This means for all modes $\vec{q}$, where the condition (35) is satisfied, the mode occupation is $\langle n_{\vec{q}} \rangle = 1/2$. Let us assume that for any two points in K there exists a path connecting both points, along which $\langle n_{\vec{k}} \rangle$ is continuous [23], and the existence of modes with $\langle n_{\vec{k}} \rangle < 1/2$. Both assumptions should be true for physically relevant models and were found to hold in all cases considered in the Kitaev model. In particular, steps in the occupation number would have to be inherited from a spectrum with steps, which is not to be expected in physical systems; small occupation numbers, however, are to be expected at least for UV modes. Then, we can set up the following chain of consequences: through the continuity condition, the existence of nonthermally occupied modes $\vec{k}^+$ with $\langle n_{\vec{k}^+} \rangle \geqslant 1/2$ implies the existence of modes $\vec{q}$ with $\langle n_{\vec{q}} \rangle = 1/2$. This in turn is equivalent to the fulfilling of the condition (35), which implies the occurrence of DQPTs in the time evolution. The mode occupation $\langle n_{\vec{k}^+} \rangle \geqslant 1/2$ is nonthermal in the sense that it cannot be realized by Fermi-Dirac statistics with positive temperature.

An equivalent formulation of condition (35) is

$$\exists \vec{q} \in K \text{ such that } \Delta_{\vec{q}}(\alpha_0)\Delta_{\vec{q}}(\alpha_1) + \epsilon_{\vec{q}}(\alpha_0)\epsilon_{\vec{q}}(\alpha_1) = 0, \tag{38}$$

where α is the quench parameter of the BCS-type Hamiltonian (see Appendix B). From this it becomes clear that after quenching to a gapless phase there are zeros of the dynamical partition function on the real time axis, since $E_{\vec{q}}(\alpha) = 0 \Leftrightarrow \epsilon_{\vec{q}}(\alpha) = \Delta_{\vec{q}}(\alpha) = 0$. In the mode occupation picture this can be interpreted as follows: when quenching to a gapless phase, excitations cost no energy; thus, any quench produces inverted mode occupation.

As discussed in the previous section, areas of zeros covering the real time axis result in jumps in the second time derivative of the dynamical free energy density if there is a jump in the density of zeros. Equation (34) gives a "layer" of zeros for every $n \in \mathbb{Z}$. Therefore, our total density of zeros is a sum of the densities of the individual "layers," $\rho_z(z) = \sum_n \rho_z^n(z)$. The single layer densities are given the Jacobi determinant of the change of variables $\vec{k} \to z_n(\vec{k})$ [22],

$$\begin{aligned}
\rho_z^n(z) &= \frac{1}{\pi^2}\begin{vmatrix} \frac{\partial \mathrm{Re}(z_n)}{\partial k_x} & \frac{\partial \mathrm{Re}(z_n)}{\partial k_y} \\ \frac{\partial \mathrm{Im}(z_n)}{\partial k_x} & \frac{\partial \mathrm{Im}(z_n)}{\partial k_y} \end{vmatrix}^{-1} \\
&= \frac{1}{\pi^2}\left[\left(\frac{\partial_{k_x} B_{\vec{k}}^2}{2E_{\vec{k}}B_{\vec{k}}^2} - \frac{\ln\left(B_{\vec{k}}^2\right)}{2E_{\vec{k}}^2}\partial_{k_x}E_{\vec{k}}\right)\left(-\frac{(2n+1)\pi}{2E_{\vec{k}}^2}\partial_{k_y}E_{\vec{k}}\right) - \left(\frac{\partial_{k_y} B_{\vec{k}}^2}{2E_{\vec{k}}B_{\vec{k}}^2} - \frac{\ln\left(B_{\vec{k}}^2\right)}{2E_{\vec{k}}^2}\partial_{k_y}E_{\vec{k}}\right)\left(-\frac{(2n+1)\pi}{2E_{\vec{k}}^2}\partial_{k_x}E_{\vec{k}}\right)\right]^{-1} \\
&= \frac{4E_{\vec{k}}^3 B_{\vec{k}}^2}{(2n+1)\pi^3}\left(\partial_{k_x}E_{\vec{k}}\partial_{k_y}B_{\vec{k}}^2 - \partial_{k_y}E_{\vec{k}}\partial_{k_x}B_{\vec{k}}^2\right)^{-1} = \frac{4E_{\vec{k}}^3 B_{\vec{k}}^2}{(2n+1)\pi^3}\begin{vmatrix} \frac{\partial E_{\vec{k}}}{\partial k_x} & \frac{\partial E_{\vec{k}}}{\partial k_y} \\ \frac{\partial B_{\vec{k}}^2}{\partial k_x} & \frac{\partial B_{\vec{k}}^2}{\partial k_y} \end{vmatrix}^{-1}, \quad \vec{k} \equiv \vec{k}(z_n).
\end{aligned} \tag{39}$$

At this point a more technical view of the zeros of the partition function is useful: the zeros $z_n(\vec{k})$ correspond to intersections of the isolines

$$B_{\vec{k}}^2 = \exp\left(\frac{(2n+1)\pi\,\mathrm{Re}[z_n(\vec{k})]}{\mathrm{Im}[z_n(\vec{k})]}\right), \quad E_{\vec{k}} = \frac{(2n+1)\pi}{2\mathrm{Im}[z_n(\vec{k})]} \tag{40}$$

in the momentum plane. This means that the density of zeros $\rho_z^n(z)$ diverges at the boundary, since there $\vec{\nabla}E_{\vec{k}} \parallel \vec{\nabla}B_{\vec{k}}^2$. Thus, when approaching the boundary of an interval T_n^* from the inside of the interval, the second time derivative of $\mathrm{Re}[f(t)]$ will diverge.

IV. DYNAMICAL PHASE TRANSITIONS IN THE KITAEV HONEYCOMB MODEL

A. Zeros of the dynamical partition function in the Kitaev model

In the Kitaev model not only quenches to the massless phase create inverted mode occupation. Also quenches across phase boundaries with final parameter $\vec{J}_1$ in a massive phase induce critical points in the real time evolution. It is physically reasonable to assume that the mode occupation number $\langle n_{\vec{k}} \rangle$ is sufficiently well behaved, namely, that for any two $\vec{k}_0$, $\vec{k}_1$ there exists a path $\vec{\gamma} : [0,1] \to [-\pi,\pi]^2$ with $\vec{\gamma}(0) = \vec{k}_0$ and $\vec{\gamma}(1) = \vec{k}_1$ such that $\langle n_{\vec{\gamma}(s)} \rangle, s \in [0,1]$, is continuous. We found this to be true for all considered cases. Under this prerequisite, the existence of a fully occupied mode $\vec{k}^+$, $\langle n_{\vec{k}^+} \rangle = 1$, implies that $\langle n_{\vec{q}} \rangle = 1/2$ somewhere, because $\langle n_{\vec{k}=0} \rangle = 0$. $\langle n_{\vec{k}^+} \rangle = 1$ corresponds to $|B_{\vec{k}^+}| = \infty$ and this happens when

$$\begin{aligned} 0 &= u_{\vec{k}^+}(\vec{J}_0) u_{\vec{k}^+}(\vec{J}_1) + v_{\vec{k}^+}(\vec{J}_0) v_{\vec{k}^+}(\vec{J}_1) \\ \wedge\, 0 &\neq u_{\vec{k}^+}(\vec{J}_0) v_{\vec{k}^+}(\vec{J}_1) - u_{\vec{k}^+}(\vec{J}_1) v_{\vec{k}^+}(\vec{J}_0). \end{aligned} \tag{41}$$

One possibility to fulfill this is

$$\pm 1 = \frac{\epsilon_{\vec{k}^+}(\vec{J}_0)}{E_{\vec{k}^+}(\vec{J}_0)} = -\frac{\epsilon_{\vec{k}^+}(\vec{J}_1)}{E_{\vec{k}^+}(\vec{J}_1)}. \tag{42}$$

Now, consider a quench ending in the x phase ($J_1^x \geqslant J_1^y + J_1^z$) and $\vec{k}^+ = (\pi,0)$. Then $\epsilon_{\vec{k}^+}(\mathbf{J}_1) = 2(J_1^z - J_1^x + J_1^y)$ and $\epsilon_{\vec{k}^+}(\vec{J}_1)/E_{\vec{k}^+}(\vec{J}_1) = -1$. We find that at this point both quenches, starting from another massive phase,

$$J_0^y < J_0^x + J_0^z \;\Rightarrow\; \frac{\epsilon_{\vec{k}^+}(\vec{J}_0)}{E_{\vec{k}^+}(\vec{J}_0)} = 1, \tag{43}$$

and from the massless phase,

$$J_0^x < J_0^y + J_0^z \;\Rightarrow\; \frac{\epsilon_{\vec{k}^+}(\vec{J}_0)}{E_{\vec{k}^+}(\vec{J}_0)} = 1, \tag{44}$$

lead to nonanalytic behavior because (42) is fulfilled in both cases. The same can be shown for quenches ending in the other massive phases; only $\vec{k}^+$ needs to be chosen appropriately. This shows that in the Kitaev model occupation inversion is produced by quenches within the massless phase or quenches crossing phase boundaries.

Figure 4 displays locations of the zeros of the Loschmidt echo in the complex plane given by Eq. (34) for two quenches, one within the A_x phase and one from the A_x phase to the massless phase. Both panels include a phase diagram with an arrow indicating the quench parameters $\vec{J}_0 \to \vec{J}_1$. The numerical values for the parameters for this figure and all following figures are listed in Table I in Appendix C. The zeros do indeed form areas, which are restricted to the left half plane for the quench within the massive phase but cover parts of the real time (imaginary z) axis when $\vec{J}_0$ and $\vec{J}_1$ lie in different phases.

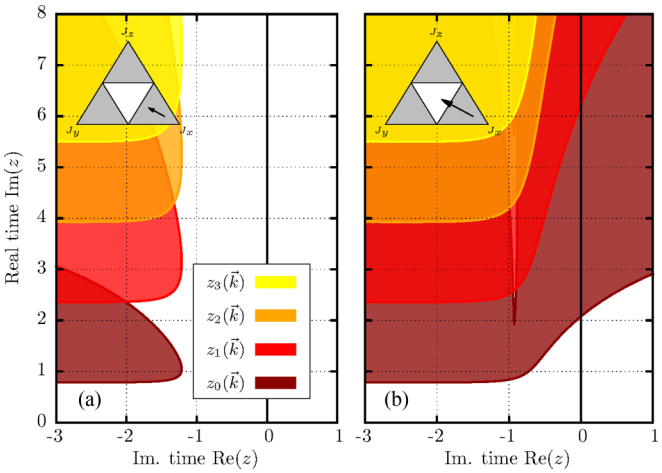

FIG. 4. (Color online) Distribution of zeros of the Loschmidt echo in the complex time plane computed according to Eq. (34) for two different quenches. The zeros form areas in the complex plane. (a) Quench within one phase. The zeros are restricted to the left half plane and no DQPTs occur. (b) Quench to the massless phase. The zero areas overlap the real time axis (i.e., imaginary z axis) and DQPTs occur at the intersections of the boundaries of the single areas $z_n(\vec{k})$ with the real time axis. Time is measured in units of $\sum_\alpha J_1^\alpha$.

B. Real time evolution

On the real time axis the rate function of the Loschmidt echo $\mathcal{L}(t) = |Z(it)|^2$ reads

$$r(t) = -\frac{1}{2\pi^2} \int_0^\pi \int_{-\pi}^\pi dk_x dk_y \times \ln\left(\frac{\sqrt{1 + 2B_{\vec{k}}^2 \cos(2E_{\vec{k}} t) + B_{\vec{k}}^4}}{1 + B_{\vec{k}}^2} \right) \tag{45}$$

and the time derivative is

$$\dot{r}(t) = \frac{1}{\pi^2} \int_0^\pi \int_{-\pi}^\pi dk_x dk_y \frac{B_{\vec{k}}^2 E_{\vec{k}} \sin(2E_{\vec{k}} t)}{1 + 2B_{\vec{k}}^2 \cos(2E_{\vec{k}} t) + B_{\vec{k}}^4}. \tag{46}$$

Figure 5 shows the time evolution of the rate function and its time derivative for various quenches obtained by numerical evaluation of the corresponding integrals. The gray-shaded areas in the plots indicate the intervals T_n^* [cf. Eq. (36)] of vanishing partition function. The results exhibit the properties expected from the previous considerations. The rate function is smooth for quenches within the gapped phases; however, nonanalyticities occur when phase boundaries are crossed in a quench or after a quench within the gapless phase. The beginning and end points of the critical intervals are equidistant, respectively, and for quenches ending in the massless phase the intervals extend to infinity. As anticipated, nonanalyticities only show up at the boundaries of the critical intervals. Moreover, the nonanalyticities emerge as discontinuities of $\ddot{r}(t)$, i.e., kinks in $\dot{r}(t)$.

Note that the two plots in panels (a) and (c) show the time evolution of the rate function after the two quenches for which Fig. 4 shows the location of the zeros of the partition function.

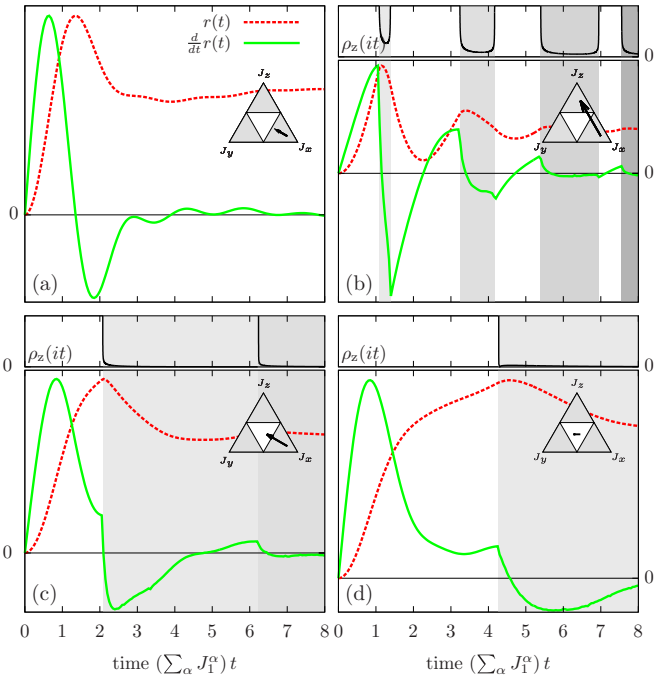

FIG. 5. (Color online) Real time evolution of the rate function of the Loschmidt echo (45) and its time derivative (46) for various quenches. Both were obtained by numerical evaluation of the integrals. The gray-shaded areas indicate sections of the real time axis that are covered by areas of vanishing Loschmidt echo (cf. Fig. 4). If zeros of the Loschmidt echo cover parts of the time axis, also the density of zeros on the time axis, $\rho_z(it)$, is included. Kinks in the time derivative of the rate function are observed when quenching across a phase boundary or within the massless phase.

C. The 1d limit

In the limit $J_\alpha \to 0$ for any $\alpha \in \{x,y,z\}$ the 2d Kitaev model (4) degenerates and becomes a set of separate 1d spin chains. Let us consider the case $J_z = 0$. The vanishing of one of the other two parameters will give the same result due to the threefold symmetry. For $J_z = 0$ the condition for nonanalyticities (35) is fulfilled at $\vec{q}$ with

$$\cos(q_x - q_y) = \frac{J_0^x J_1^x + J_0^y J_1^y}{J_0^x J_1^y + J_1^x J_0^y}. \tag{47}$$

Along this line also the spectrum is constant,

$$E_{\vec{q}} = \sqrt{J_1^{x2} + J_1^{y2} + 2J_1^x J_1^y \frac{J_0^x J_1^x + J_0^y J_1^y}{J_0^x J_1^y + J_1^x J_0^y}}. \tag{48}$$

Thus, the critical intervals T_n^* defined in Eq. (36) become critical points

$$t_n^* = \frac{(2n+1)\pi}{2E_{\vec{q}}} \equiv \frac{2n+1}{2} t^* \tag{49}$$

on the real time axis. Figure 6 shows the rate functions for two different quenches with $J_0^z = J_1^z = 0$. The quench in Fig. 6(a) does not cross a phase boundary and therefore the rate function is analytic. However, in Fig. 6(b) $\vec{J}_0 = (\frac{1}{4}, \frac{3}{4}, 0)$ and $\vec{J}_1 = (\frac{3}{4}, \frac{1}{4}, 0)$ lie in different phases, and according to Eq. (49)

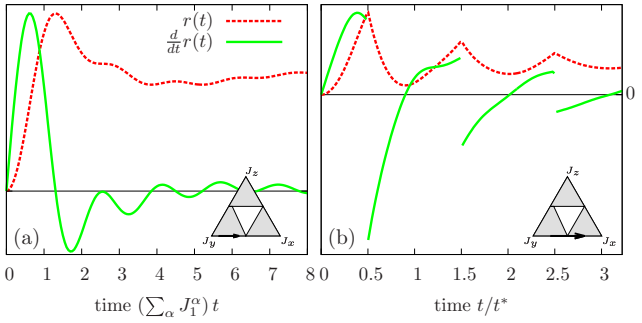

FIG. 6. (Color online) Time evolution of the rate function $r(t)$ of the Loschmidt echo and its time derivative for two quenches in the effectively one-dimensional Kitaev model with $J_z = 0$. The quench in (a) does not cross the phase boundary and the rate function is analytic. In (b) the phase boundary is crossed and discontinuities of $\dot{r}(t)$ occur at equidistant instances in time t_n^*.

there are critical times $t_n^* = \frac{2n+1}{2}\sqrt{\frac{5}{8}}\pi$ at which the rate function becomes singular. In particular, these singularities are discontinuities in the first time derivative of the rate function, not in the second as in the genuinely two-dimensional cases. This observation underlines the fact that the continuity of the first derivative is inherent to the higher dimensionality of the nondegenerate Kitaev model.

D. The long time limit

In a recent work [14] it was stated that if the Loschmidt echo $\mathcal{L}(t)$ supports analytic continuation, then the long real time limit $\lim_{t\to\infty} \mathcal{L}(t)$ and the long imaginary time limit $\lim_{\tau\to\infty} \mathcal{L}(-i\tau)$ coincide. In the context of dynamical phase transitions this gives rise to the conjecture that the occurrence of DQPTs is closely related to the long time behavior of $\mathcal{L}(t)$. Dynamical quantum phase transitions occur if the zeros of the dynamical partition function cross the real time axis. This means, $r(z)$, the rate function of the Loschmidt echo, is nonanalytic in the $\tau > 0$ half plane; therefore, the long imaginary time limit and the long real time limit do not necessarily have to coincide.

On the imaginary time axis $z = \tau$, with the eigenbasis of the quenched Hamiltonian $|\phi_n\rangle$, corresponding energies E_n, and $c_n = \langle\phi_n|\psi_i\rangle$,

$$\mathcal{L}(-i\tau) = |\langle\psi_i|e^{-H\tau}|\psi_i\rangle|^2 = \left|\sum_{n,n'} c_n^* c_{n'} e^{-E_{n'}\tau}\langle\phi_n|\phi_{n'}\rangle\right|^2$$
$$= \left|\sum_n |c_n|^2 e^{-E_n\tau}\right|^2. \tag{50}$$

Now, shifting the energy such that $E_0 = 0$ and assuming the ground state $|\phi_0\rangle$ to be nondegenerate,

$$\lim_{\tau\to\infty} \mathcal{L}(-i\tau) = |c_0|^4 = |\langle\phi_0|\psi_i\rangle|^4 = \mathcal{F}^4, \tag{51}$$

where $\mathcal{F} \equiv |\langle\phi_0|\psi_i\rangle|$ is the fidelity. Thereby, the Loschmidt echo is connected to the fidelity in the large imaginary time limit.

As the Loschmidt echo $\mathcal{L} \propto e^{-Nr(t)}$ equals zero in the thermodynamic limit, one should rather formulate Eq. (51) in terms of the rate function:

$$\lim_{\tau\to\infty} r(-i\tau) = -\lim_{\tau\to\infty}\lim_{N\to\infty}\frac{1}{N}\ln\mathcal{L}(-i\tau) = -\lim_{N\to\infty}\frac{1}{N}\ln\mathcal{F}^4. \quad (52)$$

According to the previous considerations this yields

$$\lim_{t\to\infty} r(t) = -\lim_{N\to\infty}\frac{1}{N}\ln\mathcal{F}^4 \quad (53)$$

if $r(z)$ is analytic in the $\tau > 0$ half plane. This is a quite remarkable result: In the long time limit the Loschmidt echo approaches a value given solely by the overlap of the initial state with the ground state of the postquench Hamiltonian, although the stationary state will surely never be that ground state. Quenching inevitably produces an excited state. Moreover, some information about the initial state is preserved for all times.

For the Kitaev model the fidelity is

$$\mathcal{F} = |\langle\psi_i|\phi_0\rangle| = \frac{\left|\langle 0|\prod_{\vec{k}}'(1+B_{\vec{k}}a_{-\vec{k}}a_{\vec{k}})|0\rangle\right|}{\sqrt{\langle\psi_0|\psi_0\rangle}} = \frac{1}{\sqrt{\langle\psi_0|\psi_0\rangle}} \overset{(18)}{=} \exp\left[-\frac{N}{2}\int\frac{d^2k}{4\pi^2}\ln\left(1+B_{\vec{k}}^2\right)\right]. \quad (54)$$

Thus, if the above conjecture is valid, we should find

$$\lim_{t\to\infty} r(t) = \frac{1}{2\pi^2}\int d^2k \ln\left(1+B_{\vec{k}}^2\right) \quad (55)$$

for quenches within the massive phases. Figure 7 shows the long time behavior of the rate function for a quench within the A_x phase and for a quench crossing phase boundaries; indeed, the rate function converges to the value given by the fidelity after the quench within the massive phase. In the other case, however, the rate function seems to converge, but the value it approaches differs from the one given by the fidelity. Various other cases were checked and the behavior was always consistent with above mentioned conjecture.

One can explain the convergence of the rate function heuristically based on the specific form given in Eq. (45). The expressions for the long time limit of the rate function in Eq. (55) and the definition of the rate function in Eq. (45) only differ in the nominators in the argument of the logarithm, which are 1 and $1 + B_{\vec{k}}^2 e^{-2iE_{\vec{k}}t}$, respectively. In the long time limit the factor $e^{-2iE_{\vec{k}}t}$ oscillates extremely fast as a function of $\vec{k}$. If $B_{\vec{k}}^2$ is slowly changing compared to these oscillations and also small such that

$$\ln\left(1+B_{\vec{k}}^2 e^{-2iE_{\vec{k}}t}\right) \approx B_{\vec{k}}^2 e^{-2iE_{\vec{k}}t}, \quad (56)$$

then the contributions of neighboring points in the momentum plane will cancel in the integral and therefore both integrals Eqs. (45) and (55) become equal. However, if the integrand is singular, there are areas where $|B_{\vec{k}}| \approx 1$ and therefore the contributions of close-by points do not necessarily cancel. As a result the values of the integrals differ.

In the absence of DQPTs Eq. (53) can also be derived rigorously for BCS-type models by considering the Taylor expansion of the logarithm in the integrand of Eq. (45) and computing the time averages of the single contributions in the power series.

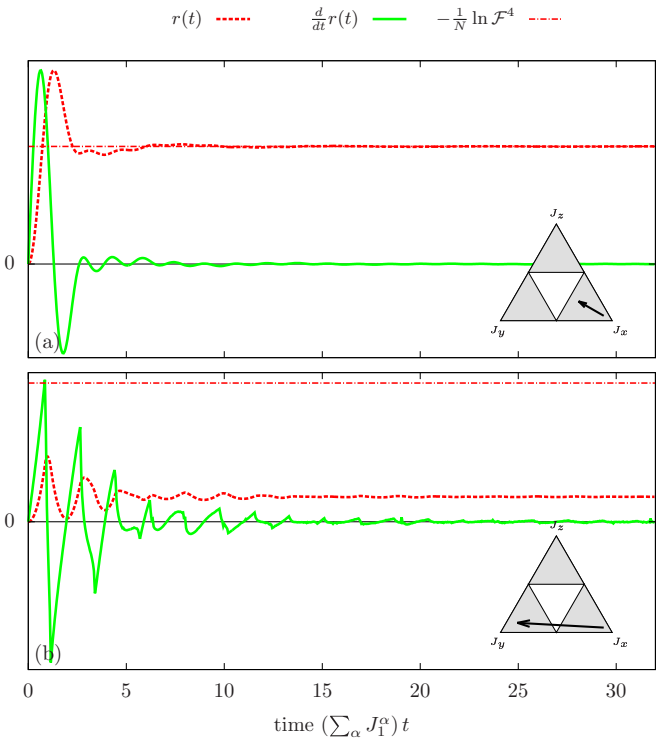

FIG. 7. (Color online) Long-time behavior of the rate function (a) after a quench within the A_x phase and (b) after a quench crossing phase boundaries. The rate function converges in both cases. For the quench within the massive phase it indeed approaches the value predicted by Heyl's and Vojta's conjecture (52), and in the other case the limit lies well off that value. Note that the derivative of the rate function converges to the zero line in both cases.

E. Ramping

It is known that dynamical quantum phase transitions also occur if the Hamiltonian parameter is continuously ramped across a critical point instead of quenching it [3]. However, it is not clear what happens after ramping the parameter within a gapless phase. In a gapless phase the adiabatic theorem does not apply and it is known that also slow ramping can produce a nonzero defect density [24]. But are these excitations sufficient to induce dynamical quantum phase transitions?

Assume the parameter $\vec{J}(t)$ of the Hamiltonian is not quenched immediately from $\vec{J}(t<0) = J_0$ to $\vec{J}(t \geqslant 0) = \vec{J}_1$, but continuously according to some protocol with $\vec{J}(t<0) = \vec{J}_0$ and $\vec{J}(t > t_r) = \vec{J}_1$. In this case, the state of the system must at any time still be of the form given in Eq. (16), because at any time $H(\vec{J}(t))$ can only excite both modes with opposite momenta $\vec{k}$, $-\vec{k}$ in one $\vec{k}$ sector. For $t > t_r$ the dynamics is the same as after a quench; however, the $B_{\vec{k}}$ will depend on the details of the ramping protocol. As discussed above $B_{\vec{k}}$ is directly related to the mode occupation number $\langle n_{\vec{k}}\rangle$. Thus, in order to determine whether DQPTs occur after ramping from $\vec{J}_0$ to $\vec{J}_1$ instead of quenching, it is sufficient to compute the mode occupation at $t = t_r$.

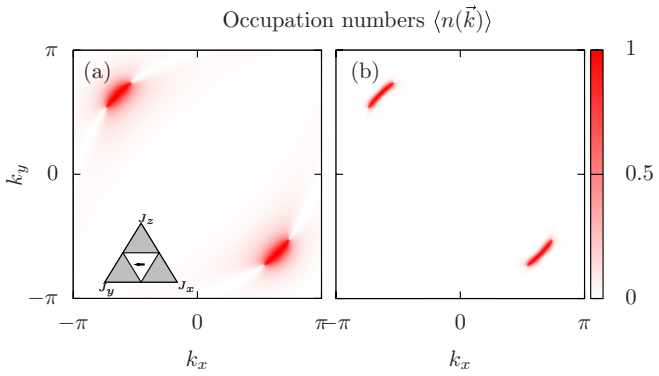

FIG. 8. (Color online) (a) Mode occupation $\langle n_{\vec{k}}\rangle$ after quenching from $\vec{J}_0$ to $\vec{J}_1$ within the gapless phase and (b) mode occupation after linearly ramping from $\vec{J}_0$ to $\vec{J}_1$ with ramping time $t_r = 50$.

In order to get the mode occupation $\langle n_{\vec{k}}\rangle$ we make use of the fact that the total time evolution is simply made up by the time evolution of independent two-level systems in the single $\vec{k}$ sectors and the corresponding Hamiltonians are

$$H_{\vec{k}}(\vec{J}(t)) = \frac{1}{2}\begin{pmatrix} \epsilon_{\vec{k}}(\vec{J}(t)) & \Delta_{\vec{k}}(\vec{J}(t)) \\ \Delta_{\vec{k}}(\vec{J}(t)) & \epsilon_{\vec{k}}(\vec{J}(t)) \end{pmatrix}. \tag{57}$$

In these terms the initial state is the ground state of $H_{\vec{k}}(\vec{J}_0)$, $H_{\vec{k}}(\vec{J}_0)|\psi_{i,\vec{k}}\rangle = -E_{\vec{k}}(\vec{J}_0)|\psi_{i,\vec{k}}\rangle$, and the time evolved state $|\psi_{\vec{k}}(t)\rangle$ can be obtained by numerical integration of the Schrödinger equation. The mode occupation number after the ramping is then given by the overlap

$$\langle n_{\vec{k}}\rangle = |\langle\psi^+_{\vec{k}}|\psi_{\vec{k}}(t_r)\rangle|^2, \tag{58}$$

where $H_{\vec{k}}(\vec{J}_1)|\psi^+_{\vec{k}}\rangle = E_{\vec{k}}|\psi^+_{\vec{k}}\rangle$.

Figure 8 shows the final occupation numbers for a quench within the gapless phase and for linear ramping with

$$\vec{J}(t) = \begin{cases} \vec{J}_0, & t < 0, \\ \vec{J}_0 + (\vec{J}_1 - \vec{J}_0)t/t_r, & 0 \leqslant t \leqslant t_r, \\ \vec{J}_1, & t > t_r, \end{cases} \tag{59}$$

and ramping period $t_r = 50$. Note that the occupation numbers remain unchanged afterwards. As expected from the previous considerations the quench produces regions of nonthermally occupied modes in the Brillouin zone. Such areas are also present after the ramping. This means that also in the time evolution for times $t > t_r$ there will be dynamical quantum phase transitions.

F. Quenching the magnetic field

In the presence of a magnetic field the phase B (cf. Fig. 2) becomes gapped and at $J_x = J_y = J_z \equiv J$ there exists a diagonal form of the Hamiltonian [15] with spectrum $E_{\vec{k}}(J,\kappa)$ as given in Eq. (13) that maps to the general two-band form (see Appendix A for details)

$$H(J,\kappa) = \sum_{\vec{k}} \vec{\gamma}^\dagger_{\vec{k}}(\vec{b}_{\vec{k}}(\alpha)\cdot\vec{\sigma})\vec{\gamma}_{\vec{k}}, \tag{60}$$

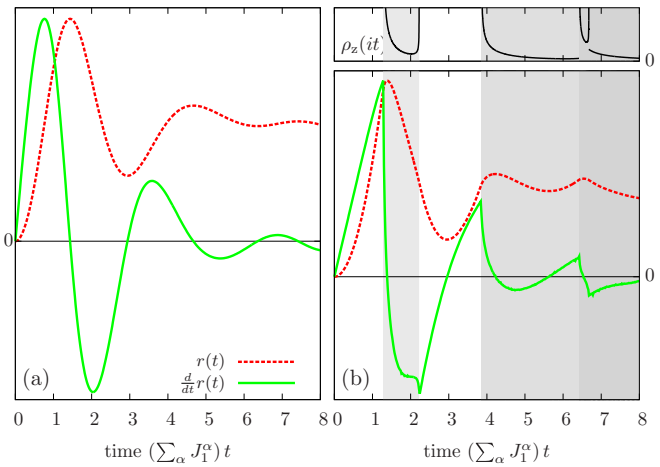

FIG. 9. (Color online) Time evolution of the rate function in the Kitaev model with additional magnetic field after quenching the magnetic field. (a) Quench within one phase, $\kappa_0 = 0.5 \to \kappa_1 = 0.1$. (b) Quench across the phase boundary, $\kappa_0 = 0.5 \to \kappa_1 = -0.1$.

where $\vec{\sigma} = (\sigma_x,\sigma_y,\sigma_z)^T$ is the vector of Pauli matrices, $\gamma^\dagger_{\vec{k}} = (d^\dagger_{\vec{k}}, d_{-\vec{k}})$, and

$$b_{\vec{k}}(J,\kappa) = \frac{1}{2}\begin{pmatrix} \mathrm{Re}[\tilde{\Delta}_{\vec{k}}(J,\kappa)] \\ \mathrm{Im}[\tilde{\Delta}_{\vec{k}}(J,\kappa)] \\ \tilde{\epsilon}_{\vec{k}}(J,\kappa) \end{pmatrix}. \tag{61}$$

The magnetic field $\vec{h}$ is contained in the parameter $\kappa \sim \frac{h_x h_y h_z}{J^2}$. It introduces topological order in the B phase, characterized by the Chern number

$$\nu(\kappa) = \frac{1}{4\pi}\int_{-\pi}^{\pi}\int_{-\pi}^{\pi} dk_x dk_y \frac{\vec{b}_{\vec{k}}\cdot(\partial_{k_x}\vec{b}_{\vec{k}}\times\partial_{k_y}\vec{b}_{\vec{k}})}{|\vec{b}|^3} = \mathrm{sgn}(\kappa). \tag{62}$$

It was demonstrated that in such systems any quench crossing the boundary between topologically distinct phases induces dynamical quantum phase transitions [7].

Figure 9 shows the time evolution of the rate function after quenching the magnetic field within one phase and between two topologically distinct phases. As expected the signature of dynamical quantum phase transitions shows up after the quench across the phase boundary.

V. CONCLUSIONS

We demonstrated how the domains of zeros in 2d BCS-type models differ qualitatively compared to 1d systems; namely, in the thermodynamic limit, the zeros coalesce to dense areas of zeros in the complex time plane rather than lines. The covering of intervals of the real time axis by such areas of zeros indicates the existence of critical points in the time evolution. We showed how this leads to dynamical quantum phase transitions as discontinuities in the second time derivative of the dynamical free energy as opposed to discontinuities in the first derivative known from 1d systems.

It was found that in the Kitaev honeycomb model dynamical quantum phase transitions occur after quenches across the

phase boundaries and after quenches within the gapless phase. It is to our knowledge the first time that DQPTs are found in a two-dimensional model after quenching without crossing an equilibrium phase boundary. In accordance with the general considerations regarding the dynamics of BCS-type systems, DQPTs in the Kitaev model show up at the boundaries of the intervals T_n^* on the time axis which are included in a domain of zeros of the partition function. At these points the DQPTs appear as kinks in the first time derivative of the rate function of the Loschmidt echo. As was shown to hold for any BCS-type model, the curvature of the free energy density diverges when the boundary of such an interval is approached from the inward.

In degenerate versions of the Kitaev model, which effectively constitute one-dimensional spin chains, already the first derivative of the rate function becomes discontinuous after quenching across a phase boundary as known from other 1d models [3]. This underlines the fact that the continuity of the first derivative is inherent to the higher dimensionality of the nondegenerate Kitaev model.

Moreover, we found for the Kitaev model that, in accordance with a conjecture concerning that matter [14], the long time stationary state of the rate function of the Loschmidt echo has a close connection to the occurrence of DQPTs: if no DQPTs occur, i.e., if the rate function is analytic in at least a half of the complex plane, the rate function approaches a value given by the fidelity. If the rate function is, however, nonanalytic, it does in general not converge to this value. The fact that the long time limit in the absence of DQPTs is given by the fidelity deserves particular notice, since the fidelity is the overlap of the initial state with the ground state of the quenched Hamiltonian, but the approached stationary state is surely an excited state.

The examination of the mode occupation numbers after ramping the parameter of the Hamiltonian instead of quenching it implies that the subsequent time evolution also exhibits dynamical quantum phase transitions. Moreover, it was demonstrated that in the presence of a magnetic field quenches between the topologically ordered phases induce dynamical quantum phase transitions, which was previously proven to be a general feature in the dynamics of topologically ordered two-band models in Ref. [7].

DQPTs were to date not observed in experiments. The Loschmidt echo $\mathcal{L}(t)$, which shows the nonanalytic behavior, is not directly connected to a quantum mechanical observable. As mentioned above, the work density was suggested as an measurable quantity, which could show the signature of DQPTs. However, the Loschmidt echo becomes exponentially small with increasing system size, whereas, strictly speaking, DQPTs occur only in the thermodynamic limit. Experimentally measuring the signature of DQPTs in work densities will therefore be very challenging. Experimental consequences of DQPTs in other quantities than the work distribution function are currently being investigated. It was shown that DQPTs are connected to time scales of the order parameter dynamics in symmetry broken systems [3]; in particular the occurrence of DQPTs is directly related to the sudden transition from monotonic to oscillatory decay of the order parameter after a quench [25]. Alternatively, the previously mentioned generalized expectation values could serve as measurable quantities [8]. Moreover, it was shown in a recent work that DQPTs in Ising spin models exhibit scaling and universality and numerical results indicate that signatures of the DQPTs can be found in the dynamics of spin correlations as power-law scaling, which is solely determined by the universality class [26]. This seems to provide a very promising opportunity for measuring DQPTs, since these quantities are accessible with current experimental techniques.

The finding of DQPTs as discontinuities in higher order derivatives in higher dimensional systems raises the question of a classification of dynamical quantum phase transitions. Canovi *et al.* [8] suggested a formalism for such a classification. They related discontinuities in generalized expectation values and coexisting solutions to a first order transition. Here, we found a discontinuity in the second derivative of the dynamical free energy density. In future work it should be investigated how the findings of discontinuities in higher derivatives of the dynamical free energy density tie in with their definition.

ACKNOWLEDGMENTS

The authors thank N. Abeling, M. Heyl, and B. Blobel for valuable discussions. S.K. acknowledges support through SFB 1073 (project B03) of the Deutsche Forschungsgemeinschaft (DFG).

APPENDIX A: BOGOLIUBOV TRANSFORMATION AND POSTQUENCH EIGENBASIS

Consider the general Hamiltonian

$$H(\alpha) = \sum_{\vec{k}} \vec{\gamma}_{\vec{k}}^{\dagger} (\vec{d}_{\vec{k}}(\alpha) \cdot \vec{\sigma}) \vec{\gamma}_{\vec{k}} \tag{A1}$$

with $\vec{\sigma}$ the vector of Pauli matrices

$$\sigma_x = \begin{pmatrix} 0 & 1 \\ 1 & 0 \end{pmatrix}, \ \sigma_y = \begin{pmatrix} 0 & -i \\ i & 0 \end{pmatrix}, \ \sigma_z = \begin{pmatrix} 1 & 0 \\ 0 & -1 \end{pmatrix}, \tag{A2}$$

and $\vec{\gamma}_{\vec{k}}$ containing the creation and annihilation operators

$$\gamma_{\vec{k}} = \begin{pmatrix} f_{\vec{k}} \\ f_{-\vec{k}}^{\dagger} \end{pmatrix}. \tag{A3}$$

For $\alpha = \vec{J}$ and $\vec{b}_{\vec{k}}(\vec{J}) = (\Delta_{\vec{k}}(\vec{J})/2, 0, \epsilon_{\vec{k}}(\vec{J})/2)$ this gives the Hamiltonian of the Kitaev model as in Eq. (5). The unitary transformation

$$\begin{pmatrix} a_{\vec{k}}^{\alpha} \\ a_{-\vec{k}}^{\alpha\dagger} \end{pmatrix} = W(\alpha) \vec{\gamma}_{\vec{k}} = \begin{pmatrix} u_{\vec{k}}(\alpha) & v_{\vec{k}}(\alpha) \\ -v_{\vec{k}}(\alpha)^* & u_{\vec{k}}(\alpha)^* \end{pmatrix} \begin{pmatrix} f_{\vec{k}} \\ f_{-\vec{k}}^{\dagger} \end{pmatrix} \tag{A4}$$

that brings the Hamiltonian (A1) into diagonal form is the Bogoliubov transformation. Plugging Eq. (A4) into Eq. (A1) and demanding that all off-diagonal terms vanish yields

$$\begin{aligned} 0 = {} & d_{\vec{k}}^z (u_{\vec{k}} v_{-\vec{k}} - u_{-\vec{k}} v_{\vec{k}}) \\ & + \left(d_{\vec{k}}^x - i d_{\vec{k}}^y\right) u_{-\vec{k}} u_{\vec{k}} + \left(d_{\vec{k}}^x + i d_{\vec{k}}^y\right) v_{-\vec{k}} v_{\vec{k}}, \end{aligned} \tag{A5}$$

where all the dependencies on α have been dropped for the sake of brevity. Since W is unitary, $u_{\vec{k}}$ and $v_{\vec{k}}$ have the general

form

$$u_{\vec{k}} = \cos\theta_{\vec{k}} e^{i\phi_{\vec{k}}}, \quad v_{\vec{k}} = \sin\theta_{\vec{k}} e^{i\psi_{\vec{k}}}. \tag{A6}$$

By choosing

$$\phi_{\vec{k}} = -\psi_{\vec{k}} = -\frac{1}{2}\arctan\left(-\frac{d^y_{\vec{k}}}{d^x_{\vec{k}}}\right) \tag{A7}$$

the equation above becomes real,

$$\begin{aligned} 0 = {} & d^z_{\vec{k}}(\sin\theta_{\vec{k}}\cos\theta_{\vec{k}} - \cos\theta_{-\vec{k}}\sin\theta_{\vec{k}}) \\ & + \left|d^{xy}_{\vec{k}}\right|(\cos\theta_{\vec{k}}\cos\theta_{-\vec{k}} - \sin\theta_{\vec{k}}\sin\theta_{-\vec{k}}), \end{aligned} \tag{A8}$$

where $d^{xy}_{\vec{k}} \equiv d^x_{\vec{k}} - i d^y_{\vec{k}}$ was introduced. Then for $a^\dagger_{-\vec{k}} = (a_{-\vec{k}})^\dagger$ to hold, $\theta_{\vec{k}}$ must be an odd function of $\vec{k}$. Thus,

$$\begin{aligned} 0 \;=\; & -d^z_{\vec{k}}\sin(2\theta_{\vec{k}}) + \left|d^{xy}_{\vec{k}}\right|\cos(2\theta_{\vec{k}}) \\ \Rightarrow \tan(2\theta_{\vec{k}}) = {} & \frac{\left|d^{xy}_{\vec{k}}\right|}{d^z_{\vec{k}}} \end{aligned} \tag{A9}$$

and this yields

$$\begin{aligned} |u_{\vec{k}}|^2 = \cos^2\theta_{\vec{k}} &= \frac{1}{2}\left(1 + \frac{\epsilon_{\vec{k}}}{E_{\vec{k}}}\right), \\ |v_{\vec{k}}|^2 = \sin^2\theta_{\vec{k}} &= \frac{1}{2}\left(1 - \frac{\epsilon_{\vec{k}}}{E_{\vec{k}}}\right). \end{aligned} \tag{A10}$$

In the end it is left to choose the signs appropriately such that $u_{\vec{k}} = u_{-\vec{k}}$ and $v_{\vec{k}} = -v_{-\vec{k}}$, e.g.,

$$\begin{aligned} u_{\vec{k}} &= e^{i\phi_{\vec{k}}}\sqrt{\frac{1}{2}\left(1 + \frac{\epsilon_{\vec{k}}}{E_{\vec{k}}}\right)}, \\ v_{\vec{k}} &= \mathrm{sgn}\left(d^x_{\vec{k}}\right)e^{-i\phi_{\vec{k}}}\sqrt{\frac{1}{2}\left(1 - \frac{\epsilon_{\vec{k}}}{E_{\vec{k}}}\right)}. \end{aligned} \tag{A11}$$

With this transformation the Hamiltonian (A1) becomes diagonal

$$H(\alpha) = \sum_{\vec{k}} \frac{E_{\vec{k}}(\alpha)}{2}\left(a^{\alpha\dagger}_{\vec{k}} a^{\alpha}_{\vec{k}} - a^{\alpha}_{-\vec{k}} a^{\alpha\dagger}_{-\vec{k}}\right) \tag{A12}$$

with $E_{\vec{k}}(\alpha) = |\vec{b}_{\vec{k}}(\alpha)|$.

To compute the quench dynamics one needs the connection of the degrees of freedom $a^{\alpha_0}_{\vec{k}}$ that diagonalize the initial Hamiltonian $H(\alpha_0)$ and the degrees of freedom $a^{\alpha_1}_{\vec{k}}$ diagonalizing the final Hamiltonian $H(\alpha_1)$. This connection is given by two subsequent Bogoliubov transformations,

$$\begin{aligned} \begin{pmatrix} a^{\alpha_1}_{\vec{k}} \\ a^{\alpha_1\dagger}_{-\vec{k}} \end{pmatrix} &= W(\alpha_1)W(\alpha_0)^\dagger \begin{pmatrix} a^{\alpha_0}_{\vec{k}} \\ a^{\alpha_0\dagger}_{-\vec{k}} \end{pmatrix} \\ &= \begin{pmatrix} U_{\vec{k}}(\alpha_0,\alpha_1) & V_{\vec{k}}(\alpha_0,\alpha_1) \\ -V_{\vec{k}}(\alpha_0,\alpha_1)^* & U_{\vec{k}}(\alpha_0,\alpha_1)^* \end{pmatrix} \begin{pmatrix} a^{\alpha_0}_{\vec{k}} \\ a^{\alpha_0\dagger}_{-\vec{k}} \end{pmatrix} \end{aligned} \tag{A13}$$

with

$$\begin{aligned} U_{\vec{k}}(\alpha_0,\alpha_1) &= u_{\vec{k}}(\alpha_1)u_{\vec{k}}(\alpha_0)^* + v_{\vec{k}}(\vec{J}_1)v_{\vec{k}}(\alpha_0)^*, \\ V_{\vec{k}}(\alpha_0,\alpha_1) &= u_{\vec{k}}(\alpha_0)v_{\vec{k}}(\alpha_1) - u_{\vec{k}}(\alpha_1)v_{\vec{k}}(\alpha_0). \end{aligned} \tag{A14}$$

Since $|\psi_i\rangle$ is the ground state of $H(\vec{J}_0)$

$$a^{\alpha_0}_{\vec{k}}|\psi_i\rangle = \left(U_{\vec{k}}(\alpha_0,\alpha_1)a^{\vec{J}_1}_{\vec{k}} - V_{\vec{k}}(\alpha_0,\alpha_1)a^{\alpha_1\dagger}_{-\vec{k}}\right)|\psi_i\rangle = 0 \tag{A15}$$

must hold. Moreover, the ground state of a BCS-type Hamiltonian has vanishing total momentum; thus,

$$\begin{aligned} |\psi_i\rangle &= \frac{1}{\mathcal{N}}\prod_{\vec{k}}{}'\left(1 + B_{\vec{k}}(\alpha_0,\alpha_1)a^{\alpha_1\dagger}_{\vec{k}}a^{\alpha_1\dagger}_{-\vec{k}}\right)|0;\alpha_1\rangle \\ &= \frac{1}{\mathcal{N}}\exp\left(\sum_{\vec{k}} B_{\vec{k}}(\alpha_0,\alpha_1)a^{\alpha_1\dagger}_{\vec{k}}a^{\alpha_1\dagger}_{-\vec{k}}\right)|0;\alpha_1\rangle, \end{aligned} \tag{A16}$$

where the coefficients $B_{\vec{k}}(\alpha_0,\alpha_1)$ are to be determined, $\mathcal{N}$ is a normalization constant, and $|0;\alpha_1\rangle$ denotes the vacuum of the postquench fermions: $a^{\alpha_1}_{\vec{k}}|0;\alpha_1\rangle = 0$. Plugging Eq. (A16) into Eq. (A15) yields

$$\begin{aligned} & \left(U_{\vec{k}}(\alpha_0,\alpha_1)a^{\alpha_1}_{\vec{k}} - V_{\vec{k}}(\alpha_0,\alpha_1)a^{\alpha_1\dagger}_{-\vec{k}}\right) \\ & \quad \times\prod_{\vec{k}'}{}'\left(1 + B_{\vec{k}'}(\alpha_0,\alpha_1)a^{\alpha_1\dagger}_{\vec{k}'}a^{\alpha_1\dagger}_{-\vec{k}'}\right)|0\rangle_{\alpha_1} \\ & = [U_{\vec{k}}(\alpha_0,\alpha_1)B_{\vec{k}}(\alpha_0,\alpha_1) - V_{\vec{k}}(\alpha_0,\alpha_1)]a^{\alpha_1\dagger}_{-\vec{k}} \\ & \quad \times\prod_{\vec{k}'\neq\vec{k}}{}'\left(1 + B_{\vec{k}'}(\alpha_0,\alpha_1)a^{\alpha_1\dagger}_{\vec{k}'}a^{\alpha_1\dagger}_{-\vec{k}'}\right)|0;\alpha_1\rangle \\ & = 0, \end{aligned} \tag{A17}$$

which holds for

$$B_{\vec{k}}(\alpha_0,\alpha_1) = \frac{V_{\vec{k}}(\alpha_0,\alpha_1)}{U_{\vec{k}}(\alpha_0,\alpha_1)} = \frac{u_{\vec{k}}(\alpha_0)v_{\vec{k}}(\alpha_1) - u_{\vec{k}}(\alpha_1)v_{\vec{k}}(\alpha_0)}{u_{\vec{k}}(\alpha_0)u_{\vec{k}}(\alpha_1) + v_{\vec{k}}(\alpha_0)v_{\vec{k}}(\alpha_1)}. \tag{A18}$$

APPENDIX B: CONDITION FOR REAL TIME ZEROS OF THE PARTITION FUNCTION

The condition $B^2_{\vec{k}} = 1$ [cf. Eq. (35)] can be rearranged as follows: We have

$$\begin{aligned} 1 = |B_{\vec{k}}| \Leftrightarrow {} & \left|\sqrt{1 + \frac{\epsilon_{\vec{k}}(\vec{J}_0)}{E_{\vec{k}}(\vec{J}_0)}}\sqrt{1 + \frac{\epsilon_{\vec{k}}(\vec{J}_1)}{E_{\vec{k}}(\vec{J}_1)}} + \mathrm{sgn}[\Delta_{\vec{k}}(\vec{J}_0)\Delta_{\vec{k}}(\vec{J}_1)]\sqrt{1 - \frac{\epsilon_{\vec{k}}(\vec{J}_0)}{E_{\vec{k}}(\vec{J}_0)}}\sqrt{1 - \frac{\epsilon_{\vec{k}}(\vec{J}_1)}{E_{\vec{k}}(\vec{J}_1)}}\right| \\ = {} & \left|\mathrm{sgn}[\Delta_{\vec{k}}(\vec{J}_1)]\sqrt{1 + \frac{\epsilon_{\vec{k}}(\vec{J}_0)}{E_{\vec{k}}(\vec{J}_0)}}\sqrt{1 - \frac{\epsilon_{\vec{k}}(\vec{J}_1)}{E_{\vec{k}}(\vec{J}_1)}} - \mathrm{sgn}[\Delta_{\vec{k}}(\vec{J}_0)]\sqrt{1 - \frac{\epsilon_{\vec{k}}(\vec{J}_0)}{E_{\vec{k}}(\vec{J}_0)}}\sqrt{1 + \frac{\epsilon_{\vec{k}}(\vec{J}_1)}{E_{\vec{k}}(\vec{J}_1)}}\right| \end{aligned}$$

$$
\begin{aligned}
&\Leftrightarrow \left(1+\frac{\epsilon_{\vec{k}}(\vec{J}_0)}{E_{\vec{k}}(\vec{J}_0)}\right)\left(1+\frac{\epsilon_{\vec{k}}(\vec{J}_1)}{E_{\vec{k}}(\vec{J}_1)}\right)+\left(1-\frac{\epsilon_{\vec{k}}(\vec{J}_0)}{E_{\vec{k}}(\vec{J}_0)}\right)\left(1-\frac{\epsilon_{\vec{k}}(\vec{J}_1)}{E_{\vec{k}}(\vec{J}_1)}\right)\\
&\quad +2\mathrm{sgn}[\Delta_{\vec{k}}(\vec{J}_0)\Delta_{\vec{k}}(\vec{J}_1)]\sqrt{\left[1-\left(\frac{\epsilon_{\vec{k}}(\vec{J}_0)}{E_{\vec{k}}(\vec{J}_0)}\right)^2\right]\left[1-\left(\frac{\epsilon_{\vec{k}}(\vec{J}_1)}{E_{\vec{k}}(\vec{J}_1)}\right)^2\right]}\\
&= \left(1+\frac{\epsilon_{\vec{k}}(\vec{J}_0)}{E_{\vec{k}}(\vec{J}_0)}\right)\left(1-\frac{\epsilon_{\vec{k}}(\vec{J}_1)}{E_{\vec{k}}(\vec{J}_1)}\right)+\left(1-\frac{\epsilon_{\vec{k}}(\vec{J}_0)}{E_{\vec{k}}(\vec{J}_0)}\right)\left(1+\frac{\epsilon_{\vec{k}}(\vec{J}_1)}{E_{\vec{k}}(\vec{J}_1)}\right)\\
&\quad -2\mathrm{sgn}[\Delta_{\vec{k}}(\vec{J}_0)\Delta_{\vec{k}}(\vec{J}_1)]\sqrt{\left[1-\left(\frac{\epsilon_{\vec{k}}(\vec{J}_0)}{E_{\vec{k}}(\vec{J}_0)}\right)^2\right]\left[1-\left(\frac{\epsilon_{\vec{k}}(\vec{J}_1)}{E_{\vec{k}}(\vec{J}_1)}\right)^2\right]}\\
&\Leftrightarrow \frac{\epsilon_{\vec{k}}(\vec{J}_0)\epsilon_{\vec{k}}(\vec{J}_1)}{E_{\vec{k}}(\vec{J}_0)E_{\vec{k}}(\vec{J}_1)}=-\mathrm{sgn}[\Delta_{\vec{k}}(\vec{J}_0)\Delta_{\vec{k}}(\vec{J}_1)]\sqrt{\left[1-\left(\frac{\epsilon_{\vec{k}}(\vec{J}_0)}{E_{\vec{k}}(\vec{J}_0)}\right)^2\right]\left[1-\left(\frac{\epsilon_{\vec{k}}(\vec{J}_1)}{E_{\vec{k}}(\vec{J}_1)}\right)^2\right]}\\
&\Rightarrow 1=\left(\frac{\epsilon_{\vec{k}}(\vec{J}_0)}{E_{\vec{k}}(\vec{J}_0)}\right)^2+\left(\frac{\epsilon_{\vec{k}}(\vec{J}_1)}{E_{\vec{k}}(\vec{J}_1)}\right)^2. \qquad \text{(B1)}
\end{aligned}
$$

Plugging this into the second last line we find the additional condition

$$\mathrm{sgn}[\Delta_{\vec{k}}(\vec{J}_0)\epsilon_{\vec{k}}(\vec{J}_0)]=-\mathrm{sgn}[\Delta_{\vec{k}}(\vec{J}_1)\epsilon_{\vec{k}}(\vec{J}_1)], \qquad \text{(B2)}$$

which allows us to write

$$1=|B_{\vec{k}}| \;\Leftrightarrow\; \left[1=\left(\frac{\epsilon_{\vec{k}}(\vec{J}_0)}{E_{\vec{k}}(\vec{J}_0)}\right)^2+\left(\frac{\epsilon_{\vec{k}}(\vec{J}_1)}{E_{\vec{k}}(\vec{J}_1)}\right)^2 \wedge -1=\frac{\mathrm{sgn}[\epsilon_{\vec{k}}(\vec{J}_1)\Delta_{\vec{k}}(\vec{J}_1)]}{\mathrm{sgn}[\epsilon_{\vec{k}}(\vec{J}_0)\Delta_{\vec{k}}(\vec{J}_0)]}\right]. \qquad \text{(B3)}$$

Plugging in $E_{\vec{k}}(J)^2=\epsilon_{\vec{k}}(J)^2+\Delta_{\vec{k}}(J)^2$ yields

$$1=|B_{\vec{k}}(J_0,J_1)| \;\Leftrightarrow\; \Delta_{\vec{k}}(\vec{J}_0)\Delta_{\vec{k}}(\vec{J}_1)+\epsilon_{\vec{k}}(\vec{J}_0)\epsilon_{\vec{k}}(\vec{J}_1)=0. \qquad \text{(B4)}$$

So, for the emergence of a nonanalyticity at a given time $t=t^*$ we get two (simplified) conditions:

$$E_{\vec{k}}(\vec{J}_1)=\frac{(2n+1)\pi}{2t^*}\equiv C^n_{t^*}, \qquad \text{(B5)}$$

$$0=\Delta_{\vec{k}}(\vec{J}_0)\Delta_{\vec{k}}(\vec{J}_1)+\epsilon_{\vec{k}}(\vec{J}_0)\epsilon_{\vec{k}}(\vec{J}_1). \qquad \text{(B6)}$$

APPENDIX C: QUENCH/RAMPING PARAMETERS

In Table I we give a summary of the quench parameters used for the figures in the main text.

TABLE I. Quench parameters.

Figure	J_0^x	J_0^y	J_0^z	J_1^x	J_1^y	J_1^z	κ_0	κ_1
4(a)	0.8	0.1	0.1	0.6	0.2	0.2	0	0
4(b)	0.8	0.1	0.1	0.4	0.3	0.3	0	0
5(a)	0.8	0.1	0.1	0.6	0.2	0.2	0	0
5(b)	0.8	0.1	0.1	0.2	0.1	0.7	0	0
5(c)	0.8	0.1	0.1	0.4	0.3	0.3	0	0
5(d)	0.4	0.3	0.3	0.3	0.4	0.3	0	0
6(a)	0.1	0.9	0.0	0.4	0.6	0.0	0	0

TABLE I. (*Continued.*)

Figure	J_0^x	J_0^y	J_0^z	J_1^x	J_1^y	J_1^z	κ_0	κ_1
6(b)	0.25	0.75	0.0	0.75	0.25	0.0	0	0
7(a)	0.9	0.05	0.05	0.6	0.2	0.2	0	0
7(b)	0.9	0.05	0.05	0.1	0.8	0.1	0	0
8(a)	0.8	0.1	0.1	0.6	0.2	0.2	0	0
8(b)	0.8	0.1	0.1	0.4	0.3	0.3	0	0
9(a)	1/3	1/3	1/3	1/3	1/3	1/3	0.5	0.1
9(b)	1/3	1/3	1/3	1/3	1/3	1/3	0.5	−0.1

[1] M. Greiner, O. Mandel, T. Esslinger, T. Hänsch, and I. Bloch, Nature (London) **415**, 39 (2002).

[2] T. Kinoshita, T. Wenger, and D. Weiss, Nature (London) **440**, 900 (2006).

[3] M. Heyl, A. Polkovnikov, and S. Kehrein, Phys. Rev. Lett. **110**, 135704 (2013).

[4] G. E. Fisher, *Lectures in Theoretical Physics*, Lectures Delivered at the Summer Institute for Theoretical Physics, Vol. 7 (University of Colorado Press, Boulder, 1965).

[5] C. Karrasch and D. Schuricht, Phys. Rev. B **87**, 195104 (2013).

[6] J. N. Kriel, C. Karrasch, and S. Kehrein, Phys. Rev. B **90**, 125106 (2014).

[7] S. Vajna and B. Dóra, Phys. Rev. B **91**, 155127 (2015).

[8] E. Canovi, P. Werner, and M. Eckstein, Phys. Rev. Lett. **113**, 265702 (2014).

[9] M. Fagotti, arXiv:1308.0277.

[10] S. Vajna and B. Dóra, Phys. Rev. B **89**, 161105 (2014).

[11] F. Andraschko and J. Sirker, Phys. Rev. B **89**, 125120 (2014).

[12] J. Budich and M. Heyl, arXiv:1504.05599.

[13] G. Torlai, L. Tagliacozzo, and G. De Chiara, J. Stat. Mech. (2014) P06001.

[14] M. Heyl and M. Vojta, arXiv:1310.6226.

[15] A. Kitaev, Ann. Phys. **321**, 2 (2006).

[16] H.-D. Chen and J. Hu, Phys. Rev. B **76**, 193101 (2007).

[17] H.-D. Chen and Z. Nussinov, J. Phys. A: Math. Theor. **41**, 075001 (2008).

[18] Here, we choose $\alpha_r = -1$ (cf. Ref. [17]), such that the result for the spectrum agrees with the result in Ref. [15] .

[19] To be precise one would have to decide how to deal with the $k_x = 0$ axis; however, this will not play any role in the later calculations.

[20] C. N. Yang and T. D. Lee, Phys. Rev. **87**, 404 (1952).

[21] I. Bena, M. Droz, and A. Lipowski, Int. J. Mod. Phys. B **19**, 4269 (2005).

[22] W. van Saarloos and D. Kurtze, J. Phys. A: Math. Gen. **17**, 1301 (1984).

[23] Assuming conventional continuity is too strong in this case, since in the Kitaev model the mode occupation number is not necessarily continuous after quenching (see Fig. 8).

[24] S. Mondal, D. Sen, and K. Sengupta, Phys. Rev. B **78**, 045101 (2008).

[25] M. Heyl, Phys. Rev. Lett. **113**, 205701 (2014).

[26] M. Heyl, arXiv:1505.02352.